# Forced convection heat transfer from solder balls on a printed circuit board using the characteristic based split (CBS) scheme

Received April 2003
Revised November 2003
Accepted May 2004

P. Nithiarasu
*Civil and Computational Engineering Centre, School of Engineering, University of Wales Swansea, Singleton Park, Swansea, UK*

N. Massarotti
*Dipartimento di Meccanica, Strutture, Ambiente e Territorio, Universit degli Studi di Cassino, Cassino, Italy*

J.S. Mathur
*Computational and Theoretical Fluid Dynamics Division, National Aerospace Laboratories, Bangalore, India*

## Abstract

**Purpose** – To numerically model forced convection heat transfer over arrays of solder balls.

**Design/methodology/approach** – The characteristic based split (CBS) scheme has been used to solve the incompressible Navier-Stokes equations on unstructured meshes.

**Findings** – The results show an increase in heat transport with increase in Reynolds numbers. A significant change in heat transfer is also noticed with change in angle of attack.

**Originality/value** – The presented results will be useful in designing cooling systems for electronic components.

**Keywords** Convection, Solder, Heat transfer

**Paper type** Research paper

## 1. Introduction

Owing to increasing demand of high density and high frequency applications, thermal design of electronic devices has become a challenging area of research. An interesting example is given by the idea to use both sides of printed circuit boards (PCB) for its cooling. The opportunity to do so is given by thermal vias, designed to increase the thermal conductivity of printed wiring boards (PWB) (Bar-Cohen *et al.*, 2001). However, the effectiveness of these systems depends not only on the heat conducted through the board, but obviously on the heat convected/radiated away from it. As the temperature of an electronic system increases, forced convection is certainly one of the best ways of cooling it.

The authors gratefully acknowledged the support of EPSRC via grant GR/R29321/01.

International Journal for Numerical Methods in Heat & Fluid Flow
Vol. 15 No. 1, 2005
pp. 73-95

0961-5539
DOI 10.1108/09615530510571967

In modern day electronic cooling and thermal design of PCB, numerical techniques are largely employed (Bar-Cohen *et al.*, 2001; Nakayama *et al.*, 2001; Watson *et al.*, 2001; Shidore *et al.*, 2001). Most of the numerical simulations available are performed using commercial codes. However, as the geometries involved in this type of applications become more complicated, commercial codes show deficiencies in achieving accuracy and speed. For this reason simplified models have been usually employed, which are inadequate to predict heat transfer with necessary accuracy. An interesting way to approximate the flow through an electronic device is to approximate the device as a porous medium and to look at the overall heat transferred from the medium to the fluid (Zhao and Lu, 2002; Heindel *et al.*, 1996). However, this approach has not been characterized properly and more work is needed to understand the comparison between macroscopic and microscopic approaches to the solution of porous medium flows (Nakayama and Kuwahara, 2000). In the meantime, the latest developments in numerical schemes for the solution of the complete Navier-Stokes equations can be employed to improve the thermal design of electronic packaging. Recently, a fully explicit version of the well known characteristic-based-split (CBS) algorithm has been proposed by the authors for the solution of isothermal flow problems (Nithiarasu, 2003; Nithiarasu *et al.*, 2004). In this form the algorithm was proved to be accurate and efficient on unstructured meshes. In fact, for three-dimensional problems, such as those encountered in the present study, the unstructured mesh based explicit CBS solver is an excellent choice. Although structured and semi-unstructured meshes are widely employed in the solution of incompressible flows, the use of unstructured meshes is inevitable if the geometry is really complex.

The unstructured mesh methods are very well developed for compressible flows and several schemes are around for small and large scale calculations (Zienkiewicz and Taylor, 2000; Löhner, 2001). The success of these schemes is partially due to explicit time discretization of the equations along with dual time stepping methods. Extra additional dissipation to treat oscillations is generally part of these schemes. Several such schemes perform well with very high speeds but inefficient for low speed flows. Therefore often alternate schemes have been developed to solve incompressible low speed flows. The projection and velocity correction schemes are such methods designed to solve low speed incompressible flows (Chorin, 1967; Gresho and Sani, 1999; Comini and Giudice, 1972; Ramaswamy *et al.*, 1992). However, many of the projection and velocity correction schemes require some form of implicit solution to the pressure Poisson equation. Explicit CBS scheme, however, avoids the solution of matrices arising from the discretization of Poisson type equations by introducing the artificial compressibility (AC) concept together with velocity correction (Nithiarasu, 2003). The objective of the present work is to explain in detail the steps involved in the explicit CBS scheme for non-isothermal incompressible flow problems and to employ the scheme to solve a complicated problem of forced convection heat transfer from solder balls mounted on a circuit board. The analysis is presented for different Reynolds numbers within the laminar flow regime and different directions of the flow approaching the heat sources.

In Section 2, the Navier-Stokes equations in their conservation form are presented followed by Section 3, which describes the fully explicit CBS scheme for non-isothermal flow problems. In Section 4, some important features of the fully explicit scheme, including the calculation of AC parameter, are explained. The validation of the three-dimensional non-isothermal model is given in Section 5 for forced convection heat

transfer from a single hot sphere placed in a cold stream of air. The results of forced convection heat transfer from a cluster of hot solder balls are presented in Section 6. Finally, section 7 concludes the present study.

## 2. The Navier-Stokes equations

Fluid flow through electronic systems can be accurately described using the Navier-Stokes equations for incompressible non-isothermal Newtonian flow. These equations in a Cartesian domain can be written in non-dimensional conservative form, for forced convection problems as

$$\frac{\partial \mathbf{W}}{\partial t} + \frac{\partial \mathbf{F_i}}{\partial x_i} - \frac{\partial \mathbf{G_i}}{\partial x_i} = 0 \tag{1}$$

where

$$\mathbf{W} = \begin{pmatrix} \rho \\ \rho u_1 \\ \rho u_2 \\ \rho u_3 \\ \rho T \end{pmatrix}, \qquad \mathbf{F_i} = \begin{pmatrix} \rho u_j \\ \rho u_1 u_i \\ \rho u_2 u_i \\ \rho u_3 u_i \\ \rho T u_i \end{pmatrix}, \qquad \mathbf{G_i} = \begin{pmatrix} 0 \\ \tau_{1i} + p\delta_{1i} \\ \tau_{2i} + p\delta_{2i} \\ \tau_{3i} + p\delta_{3i} \\ \frac{1}{\mathrm{RePr}} \frac{\partial T}{\partial x_i} \end{pmatrix}$$

The above set of equations state the conservation of mass, momentum and energy, respectively. It should be noted here that the body forces acting on the fluid are assumed to be negligibly small in comparison with the inertial and viscous forces. In the model presented, neither thermal viscous dissipation due to the external forces nor body forces have been considered.

The non-dimensional form of deviatoric stress in the momentum equation, according to the assumption of newtonian fluid, is

$$\tau_{ij} = \frac{1}{\mathrm{Re}} \left( \frac{\partial u_i}{\partial x_j} + \frac{\partial u_j}{\partial x_i} - \frac{2}{3} \frac{\partial u_k}{\partial x_k} \delta_{ij} \right)$$

where $\delta_{ij}$ represents the Kroneker delta. In all the above equations, the following scales have been employed to obtain the non-dimensional form

$$x_i = \frac{x_i^*}{L}, \quad u_i = \frac{u_i^*}{u_\infty}, \quad p = \frac{p^*}{\rho u_\infty^2}, \quad t = \frac{t^* u_\infty}{L}, \tag{2}$$

$$T = \frac{T^* - T_c^*}{T_h^* - T_c^*}, \quad \mathrm{Re} = \frac{u_\infty L}{\nu}; \quad \mathrm{Pr} = \frac{\nu}{\alpha} \tag{3}$$

where an asterisk is used for the dimensional variables, $\alpha$ is the thermal diffusivity of the fluid, $\nu$ its kinematic viscosity, $\rho$ its density, $x_i$ the position vector components, $t$ the time, $u_i$ the velocity components, $p$ the pressure and $T$ the temperature of the fluid, $T_h^*$ and $T_c^*$ are, respectively, the hot and cold reference temperatures, $L$ the characteristic

length of the problem considered, and $u_\infty$ is a reference velocity. The non-dimensional parameters Re and Pr represent the Reynolds and Prandtl numbers, respectively.

It should be pointed out here that for incompressible flows, the density variation is small and therefore, the conservation of mass turns into an equation satisfied by divergence free velocity field. However, in the AC form of the algorithm a fictitious form of density variation is retained in the continuity equation to solve the equations fully explicitly.

## 3. The CBS scheme

In this section, the CBS scheme is briefly discussed. As mentioned earlier the explicit form of the algorithm is employed in this paper. The fully explicit form needs no simultaneous solution to the equations arising from matrices and it is much easier to handle than the semi-implicit forms. However, for problems with large source type terms, the present fully explicit form often does not give reasonable solution and semi-implicit form is necessary in such situations.

We now describe the CBS algorithm and its application to the solution of three-dimensional incompressible non-isothermal flow problems. We first define the mass flow fluxes as

$$U_j \equiv \rho u_j \tag{4}$$

rewrite the equation for mass conservation in the form

$$\frac{\partial \rho}{\partial t} = \frac{1}{c^2}\frac{\partial p}{\partial t} = -\frac{\partial U_j}{\partial x_j} \tag{5}$$

where $c$ is the speed of the acoustic wave in the fluid considered. The momentum conservation and the energy equations become, respectively,

$$\frac{\partial U_i}{\partial t} = -\frac{\partial}{\partial x_j}(U_i u_j) - \frac{\partial p}{\partial x_i} + \frac{\partial \tau_{ij}}{\partial x_j} \tag{6}$$

and

$$\frac{\partial}{\partial t}(\rho T) = -\frac{\partial}{\partial x_j}(\rho T u_j) + \frac{\partial}{\partial x_j}\left(\frac{1}{\mathrm{RePr}}\frac{\partial T}{\partial x_j}\right) \tag{7}$$

Note that for incompressible flows the acoustic wave travels at a very high speed and therefore $c^2 \rightarrow \infty$ in equation (5). However, in AC schemes, an artificial finite value of $c^2$ may be used and generally calculated from velocity and temperature fields (Nithiarasu, 2003; Malan *et al.*, 2002).

The basic idea behind the CBS scheme comes from the split procedure devised by Chorin (1967). However, the time discretization using a characteristic-Galerkin procedure leads to the following equation in which the stabilizing terms appear (Zienkiewicz and Taylor, 2000).

$$U_i^{n+1} - U_i^n = \Delta t\left[-\frac{\partial}{\partial x_j}(U_i u_j)^n - \frac{\partial p^{n+\theta_2}}{\partial x_i} + \frac{\partial \tau_{ij}^n}{\partial x_j}\right] + \frac{\Delta t^2}{2} u_k \frac{\partial}{\partial x_k}\left(\frac{\partial}{\partial x_j}(U_i u_j) + \frac{\partial p}{\partial x_i}\right)^n$$

where the pressure term is evaluated at a time $t^n + \theta_2 \Delta t$ and is given by

$$\frac{\partial p^{n+\theta_2}}{\partial x_i} \equiv \theta_2 \frac{\partial p^{n+1}}{\partial x_i} + (1 - \theta_2) \frac{\partial p^n}{\partial x_i} \tag{8}$$

where $0 \leq \theta_2 \leq 1$ ($\theta_2 = 0$ for the fully explicit form of the scheme, while $\theta_2 > 0$ for the semi-implicit form).

At this point the splitting procedure is introduced to obtain a fictitious momentum equation by dropping the pressure terms. The solution of this equation represents the first step of the algorithm. In the second step the pressure term is evaluated from a pressure continuity equation. Using the calculated pressure, the intermediate velocities obtained in the first step are corrected in the third step. For thermal flow problems, such as the one considered in this work, the temperature is calculated in the fourth step of the algorithm, as described below.

The calculation of the intermediate velocity is obtained in the first step from the solution of the equation:

$$U_i^* - U_i^n = \Delta t \left[ -\frac{\partial}{\partial x_j}(U_i u_j) + \frac{\partial \tau_{ij}}{\partial x_j} \right]^n + \frac{\Delta t^2}{2} \left[ u_k \frac{\partial}{\partial x_k} \left( \frac{\partial}{\partial x_j}(U_i u_j) \right) \right]^n \tag{9}$$

These velocities are corrected in the third step of the algorithm represented by the equation:

$$U_i^{n+1} - U_i^* = \Delta t \frac{\partial p^n}{\partial x_i} + \frac{\Delta t^2}{2} u_k \frac{\partial}{\partial x_k} \left( \frac{\partial p^n}{\partial x_i} \right) \tag{10}$$

note that $\theta_2 = 0$ for the explicit scheme. The second-order terms in the above equation are presented to show the consistency of the present scheme. However, past experience shows that the second-order term in equation (10) has very little effect on the stability and accuracy of the CBS scheme. The pressure term in the above equation is calculated in the second step of the algorithm, which can be obtained from equation (5), and rewritten as

$$\left( \frac{1}{c^2} \right)^n (p^{n+1} - p^n) = -\Delta t \frac{\partial U_i^{n+\theta_1}}{\partial x_i}. \tag{11}$$

However, $U_i^{n+\theta_1} = \theta_1 U_i^{n+1} + (1 - \theta_1) U_i^n$ where $0.5 \leq \theta_1 \leq 1$, and using equation (10) the following expression is obtained

$$U_i^{n+\theta_1} = \theta_1 \left[ U_i^* - \Delta t \frac{\partial p^n}{\partial x_i} \right] + (1 - \theta_1) U_i^n \tag{12}$$

which can then be substituted in equation (11) that represents the second step of the algorithm

$$\left( \frac{1}{c^2} \right)^n (p^{n+1} - p^n) = -\Delta t \left[ \theta_1 \frac{\partial U_i^*}{\partial x_i} + (1 - \theta_1) \frac{\partial U_i^n}{\partial x_i} \right] + \frac{\Delta t^2}{2} \theta_1 \left[ \frac{\partial^2 p^n}{\partial x_i \partial x_i} \right] \tag{13}$$

In the fourth step of the algorithm, the temperature field is calculated from the energy conservation equation disctretized in time using the same characteristic-Galerkin

procedure employed for the momentum equation. The semi-discrete form of the equation is

$$T^{n+1} - T^n = \Delta t\left[-\frac{\partial}{\partial x_i}(Tu_i)^n + \frac{\partial}{\partial x_i}\left(\frac{1}{\mathrm{RePr}}\frac{\partial T^n}{\partial x_i}\right)\right] + \frac{\Delta t^2}{2}u_k\frac{\partial}{\partial x_k}\left[\frac{\partial}{\partial x_i}(Tu_i)^n\right] \quad (14)$$

The above semi-discrete equations can now be approximated in space using the standard Galerkin finite element procedure. Further details on the CBS scheme, especially the semi- and quasi-implicit schemes, can be found in several other published works (Zienkiewicz and Taylor, 2000; Nithiarasu *et al.*, 2004; Nithiarasu, 2002, 2003; Massarotti *et al.*, 1998).

*3.1 Spatial discretization*

The computational domain is subdivided into a mesh of tetrahedral elements. Within an element each variable is approximated by a linear function, which can be expressed in terms of the variable value at each of the three nodes of the element:

$$\phi = \sum_{n=1}^{4} N_n\bar{\phi}_n = \mathbf{N}\phi \quad (15)$$

where $N_n$ are the shape functions at each node $n$ and $\bar{\phi}_n$ is the value of the generic unknown $\phi$ (p, $U_i$, and T) at the node $n$. Using the Galerkin procedure, the weak form of the governing equations is obtained by weighting each of the conservation equations by the same shape functions introduced above.

Step 1: weak form of the intermediate velocity equation

$$\int_\Omega \mathbf{N}^T\left(U_i^* - U_i^n\right)\mathrm{d}\Omega = \Delta t\left[-\int_\Omega \mathbf{N}^T\frac{\partial}{\partial x_j}(U_iu_j)\,\mathrm{d}\Omega - \int_\Omega \frac{\partial \mathbf{N}^T}{\partial x_j}\tau_{ij}\,\mathrm{d}\Omega\right]^n - \frac{\Delta t^2}{2}\left[\int_\Omega \frac{\partial}{\partial x_j}(u_j\mathbf{N}^T)\left(\frac{\partial u_jU_i}{\partial x_j}\right)\mathrm{d}\Omega\right]^n + \Delta t\left[\int_\Omega \mathbf{N}^T t_i^* n_i\,\mathrm{d}\Gamma\right]^n \quad (16)$$

where $\Omega$ refers to the entire computational domain and $\Gamma$ to its boundary. In the above equation $t_i^*$ indicates the part of the traction corresponding to the deviatoric stress while $n_i$ are the components of the outward normal to the boundary $\Gamma$. Higher order derivative terms, obtained from the integration by parts of the stabilization terms are neglected.

Step 2: weak form of the pressure equation

$$\int_\Omega \mathbf{N}^T\left(\frac{1}{\beta^2}\right)^n(p^{n+1}-p^n)\mathrm{d}\Omega = \Delta t\int_\Omega \theta_1\frac{\partial \mathbf{N}^T}{\partial x_i}\left(U^*_i - U_i^n - \Delta t\frac{\partial p^n}{\partial x_i}\right) + \int_\Omega \mathbf{N}^T\frac{\partial U_i^n}{\partial x_i}\mathrm{d}\Omega - \Delta t\left[\theta_1\int_\Gamma \mathbf{N}^T\left(U^*_i - U_i^n - \Delta t\frac{\partial p^n}{\partial x_j}\right)n_i\mathrm{d}\Gamma\right] \quad (17)$$

in which terms multiplying $\theta_1$ are integrated by parts, and the artificial parameter $\beta$ replaces the speed of sound $c$ of the governing equations.

Step 3: weak form of the velocity correction equation

$$\int_{\Omega} \mathbf{N}^T \left( U_i^{n+1} - U_i^* \right) \mathrm{d}\Omega = -\Delta t \left[ \int_{\Omega} \mathbf{N}^T \frac{\partial \mathbf{N}^T}{\partial x_i} (p^n \, \mathrm{d}\Omega) \right] + \int_{\Gamma} \mathbf{N}^T t_i^{**} n_i \, \mathrm{d}\Gamma \tag{18}$$

Note that the second-order pressure terms are neglected in the above equation to save computational time. In equation (18), boundary integral includes the traction corresponding to the pressure term that was removed from the first step.

Step 4: weak form of the energy equation

$$\begin{aligned} \int_{\Omega} \mathbf{N}^T (T^{n+1} - T^n) \mathrm{d}\Omega = & -\Delta t \left[ \int_{\Omega} \mathbf{N}^T \frac{\partial}{\partial x_i} (u_i T) \mathrm{d}\Omega + \int_{\Omega} \frac{1}{\mathrm{RePr}} \frac{\partial \mathbf{N}^T}{\partial x_i} T \mathrm{d}\Omega \right]^n \\ & - \frac{\Delta t^2}{2} \left[ \int_{\Omega} \frac{\partial}{\partial x_i} (u_i \mathbf{N}^T) \left( \frac{\partial u_i T}{\partial x_i} \right) \mathrm{d}\Omega \right]^n + \Delta t \left[ \int_{\Gamma} \mathbf{N}^T q_i n_i \mathrm{d}\Gamma \right]^n \end{aligned} \tag{19}$$

where $q_i$ represents the non-dimensional heat flux. The other boundary terms in the equation above are derived from the integration by parts of the second-order derivatives in the partial differential equations.

*3.2 Solution procedure*

The equivalent system of algebraic equations is obtained by substituting the approximated dependent variables in the weak form of the conservation equations. The resulting system of algebraic equations can be written in a matrix form as

Step 1: discretized intermediate velocity equation

$$\mathbf{M}\left( \mathbf{U}_i^* - \mathbf{U}_i^n \right) = -\Delta t [(\mathbf{C}\mathbf{U}_i + \mathbf{K}_\tau \mathbf{U}_i - \mathbf{f}) - \Delta t (\mathbf{K}_u \mathbf{u}_i)]^n \tag{20}$$

Step 2: discretized pressure equation

$$\mathbf{M}_p (\mathbf{p}^{n+1} - \mathbf{p}^n) = \Delta t \left[ \mathbf{G}\left( (1 - \theta_1) \mathbf{U}_i^n - \theta_1 \mathbf{U}_i^* \right) - \theta_1 \mathbf{H}\mathbf{p}^n - \mathbf{f}_p^n \right] \tag{21}$$

Step 3: discretized velocity correction equation

$$\mathbf{M}\mathbf{U}_i^{n+1} = \mathbf{M}\mathbf{U}_i^* - \Delta t \mathbf{G}\mathbf{p}^n \tag{22}$$

Step 4: discretized energy equation

$$\mathbf{M}\mathbf{T}^{n+1} = \mathbf{M}\mathbf{T}^n - \Delta t [\mathbf{C}\mathbf{T} - \mathbf{H}_\mathbf{T}\mathbf{T} + \mathbf{f}_T + \Delta t \mathbf{K}_u \mathbf{T}]^n \tag{23}$$

where

$$\mathbf{M} = \int_\Omega \mathbf{N}^T \mathbf{N}\, d\Omega \quad \mathbf{M}_p = \int_\Omega \mathbf{N}^T \left(\frac{1}{\beta^2}\right)^n \mathbf{N}\, d\Omega \quad \mathbf{C} = \int_\Omega \mathbf{N}^T (\nabla(u\mathbf{N}))\, d\Omega$$

$$\mathbf{f} = \int_\Gamma \mathbf{N}^T t_i^* d\Gamma \quad \mathbf{f_p} = \Delta t \theta_1 \int_\Gamma \mathbf{N}^T \left(\mathbf{U}_i^* - \mathbf{U}_\mathbf{i}^n - \Delta t \nabla \mathbf{p}^n\right) \mathbf{n}^T\, d\Gamma$$

$$\mathbf{f_T} = \Delta t \int_\Gamma \mathbf{N}^T \mathbf{q}_i\, d\Gamma \quad \mathbf{G} = \int_\Omega (\nabla \mathbf{N}^T)^T \mathbf{N}\, d\Omega \quad \mathbf{H} = \int_\Omega (\nabla \mathbf{N}^T)^T \nabla \mathbf{N}\, d\Omega$$

$$\mathbf{H_T} = \int_\Omega \frac{1}{\mathrm{RePr}} (\nabla \mathbf{N}^T)^T \nabla \mathbf{N}\, d\Omega \quad \mathbf{K_u} = \frac{1}{2} \int_\Omega (\nabla^T (\mathbf{uN}))^T (\nabla^T (\mathbf{uN}))\, d\Omega$$

$$\mathbf{K}_\tau = \int_\Omega \mathbf{B}^T \frac{1}{\mathrm{Re}} \left(I_0 - \frac{2}{3} \mathbf{m}\mathbf{m}^T\right) d\Omega$$

In above set of matrices, **B** is given as:

$$\mathbf{B} = \mathbf{SN} \tag{24}$$

where **S** is an appropriate strain matrix or operator deduced from equation (Zienkiewicz and Taylor, 2000). For a general three-dimensional problem **m** and **B** are given as

$$\mathbf{m} = \begin{bmatrix} 1 \\ 1 \\ 1 \\ 0 \\ 0 \\ 0 \end{bmatrix}, \qquad \mathbf{B} = \begin{bmatrix} 2 & & & & & \\ & 2 & & & & \\ & & 2 & & & \\ & & & 1 & & \\ & & & & 1 & \\ & & & & & 1 \end{bmatrix}$$

It is important to remark here that equal order interpolation functions are employed for all field variables.

## 4. Fully explicit scheme

As mentioned before, the fully explicit form of the CBS algorithm is obtained by substituting $\theta_2 = 0$ and $\frac{1}{2} \leq \theta_1 \leq 1$ into equation (13). At this point it becomes necessary to solve equation (13) explicitly, and therefore, $c$ needs to be replaced by an AC parameter $\beta$ as given in equations (17) and (21). In general, $\beta$ is calculated from local velocity and temperature distribution and mesh size. This gives a critical time step $\Delta t = h/(\beta + |u|)$, where $h$ is the local element size.

### *4.1 AC parameter $\beta$ and local time step*

In order to cover the whole spectrum of flow conditions encountered incompressible flow domain, it is essential to define a value of $\beta$ which is not only suitable for different Reynolds numbers, but should also take care of different flow regimes (diffusion and convection dominated) that may appear in the domain at a particular Reynolds

number. As the $\beta$ value is local, an appropriate local time step is needed to account the local stability limits. It is therefore essential to include the local time step calculations as part of the scheme.

In this work, the following relations for $\beta$ and $\Delta t$ were found appropriate for faster and accurate solutions (Nithiarasu, 2003; Nithiarasu *et al.*, 2004)

$$\beta = \max(\varepsilon, v_{\text{conv}}, v_{\text{diff}}, v_{\text{therm}}) \tag{25}$$

where $\varepsilon$ is a constant (taken as 0.5 in this study), $v_{\text{conv}}$ is the convective velocity, $v_{\text{diff}}$ is the diffusion velocity and $v_{\text{therm}}$ is the thermal velocity. These velocities can be calculated from the following non-dimensional relations

$$v_{\text{conv}} = \sqrt{u_i u_i} \tag{26}$$

$$v_{\text{diff}} = \frac{2}{h\text{Re}} \tag{27}$$

$$v_{\text{therm}} = \frac{1}{\text{RePr}h} \tag{28}$$

where $h$ is the local element size, Re is the Reynolds number and Pr is the Prandtl number. It should be noted that for pre-conditioned AC schemes, the convection and diffusion velocities are calculated differently (Malan *et al.*, 2002).

The local element size at a node $i$ is defined as

$$h_i = \min(3\text{Volume}/\text{Opposite face area})_{ie} \tag{29}$$

in three-dimensional cases (four noded tetrahedral elements). In the above equation, the minimum value is selected among the number of elements, *ie*, connected to node *i*.

The local time step $\Delta t$ is calculated as (in terms of non-dimensional quantities)

$$\Delta t = \frac{h}{u_{\text{conv}} + \beta} \tag{30}$$

The calculated $\Delta t$ that is multiplied by a safety factor varying between 0.5 and 2.0 depends on the problem and mesh used. It is important to note that this is the only parameter tuned in the present study.

## 5. Heat transfer from a single hot sphere

In this section, the developed CBS-AC scheme is validated for heat transfer analysis on a problem of forced convection from a hot sphere. This problem presents several aspects that still challenge researchers, and has been widely investigated both experimentally and theoretically (Whitaker, 1983; Clift *et al.*, 1978; Feng and Michaelides, 2000; Dandy and Dwyer, 1990; Yuge, 1960).

The flow behind a single sphere in a uniform stream becomes unsteady as the Reynolds number based on the sphere's diameter exceeds 250. However, for smaller Re, a recirculation zone appears behind the sphere when the Reynolds number is over 20.

In order to solve the problem of forced convection from a hot sphere, a single sphere is assumed to be placed in a rectangular domain of 25 diameters in length. The centre of the sphere is assumed to be located at 5 diameters from the centre line of the side boundaries along the flow and from the inlet. The centre of the sphere is therefore 20

diameters away from the exit of the channel. The sphere is assumed to be hotter than that of the air flowing into the domain and no-slip velocity boundary conditions are imposed on the sphere surface. An uniform flow is assumed at the inlet. Far field boundary conditions are imposed to the lateral sides of the channel while no boundary conditions are specified at the exit of the channel.

The results, obtained after the necessary mesh sensitivity analysis, are presented in terms of the heat and fluid flow quantities of interest in Table I. The speed and accuracy of the CBS-AC scheme are discussed in detail by Nithiarasu (2003) and not presented here for the sake of brevity.

The calculation of the average Nusselt number, Nu, has been performed according to the procedure described in Section 6. Table I presents the average Nusselt number on the sphere surface for different Reynolds numbers. The results are compared to those obtained using the experimental (Yuge, 1960; Whitaker, 1983) and numerical (Feng and Michaelides, 2000) procedures. The agreement between the present and existing results are excellent. Plate 1 shows the isotherm distribution in the vicinity of the sphere at a Reynolds number of 200.

In Figure 1, coefficient of pressure, $C_p$, values calculated along the symmetry plane in the flow direction is compared with those available from the literature (Rimon and

**Table I.**
Forced convection from a hot sphere. Average Nusselt number distribution for different Reynolds numbers

| Re | Yuge (1960) | Whitaker (1983) | Feng and Michaelides (2000) | Present |
|---|---|---|---|---|
| 50 | 5.4860 | 5.1764 | 5.4194 | 5.0678 |
| 100 | 6.9300 | 6.6151 | 6.9848 | 6.4693 |
| 200 | 8.9721 | 8.7219 | 9.1901 | 8.4943 |

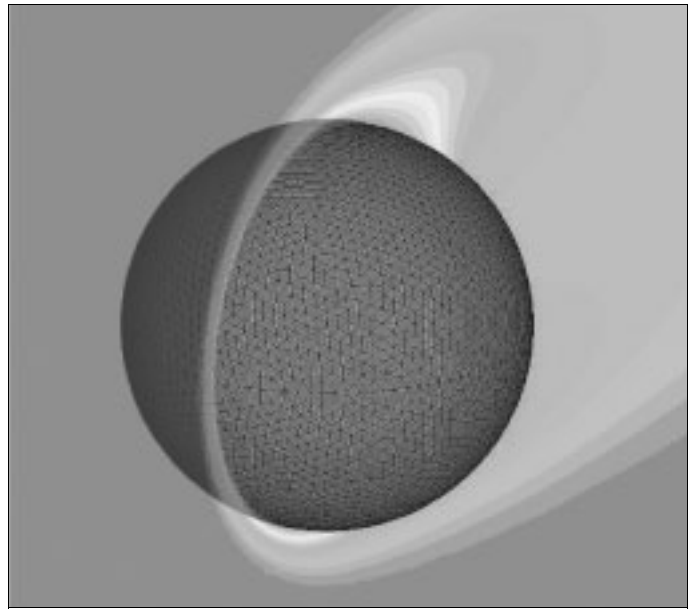

**Plate 1.**
Isotherms and surface mesh near the surface of the sphere

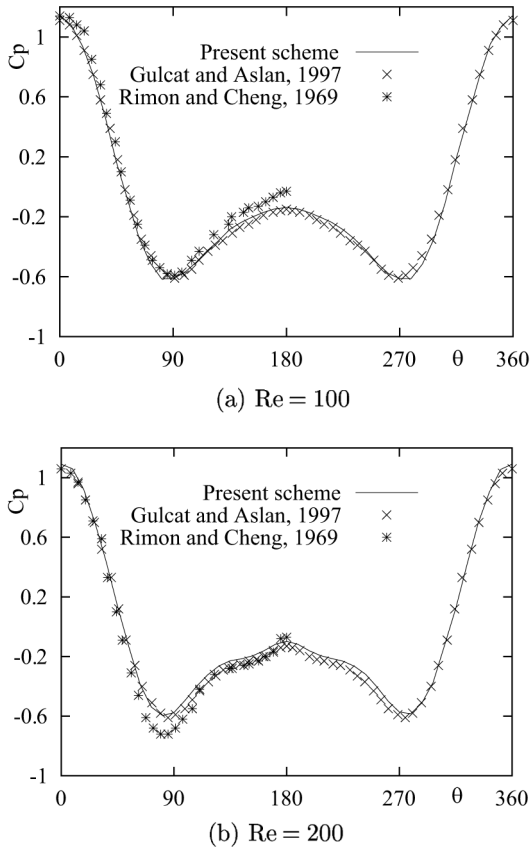


**Figure 1.**
A comparison of the coefficient of pressure, $C_p$, for different Reynolds numbers

Cheng, 1969; Gülçat and Aslan, 1997) for two different values of the Reynolds number. As seen an excellent agreement between the present and literature results has been obtained.

## 6. Forced convection heat transfer from solder balls

The problem considered in this section concerns the simulation of heat and fluid flow over an array of hot spherical solids resembling solder balls attached to a PCB. Two different arrangements, 25 in-line (5 equally spaced) and 41 staggered partial spheres are considered. The solder balls are considered to be partial spheres, whose centres lie on the horizontal plane (*x-z*) as shown in Figure 2. These solder ball arrangement is obtained by cutting the spheres with the horizontal wall (board) on which the balls are placed. The diameter of the spheres is considered to be equal to one, and the distance between the ball centres and the plane that represents the circuit board is equal to 0.35, as can be evinced from Figure 2(a). The same figure shows an example of the staggered arrangement considered (Figure 2(b)). This staggered arrangement is obtained by introducing another sphere at the centre of the space between four in-line spheres.

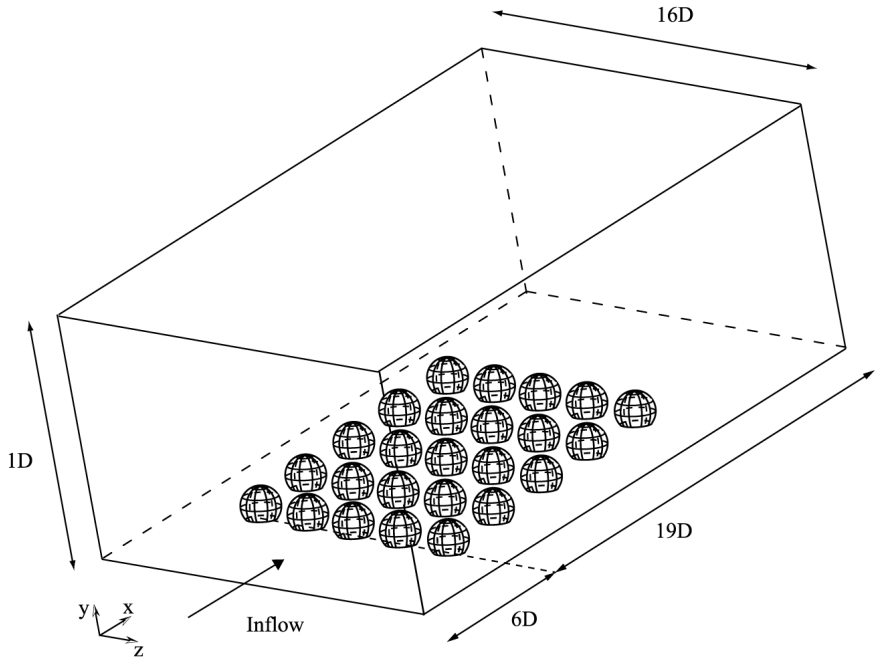


(a) Problem definition for in-line arrangement

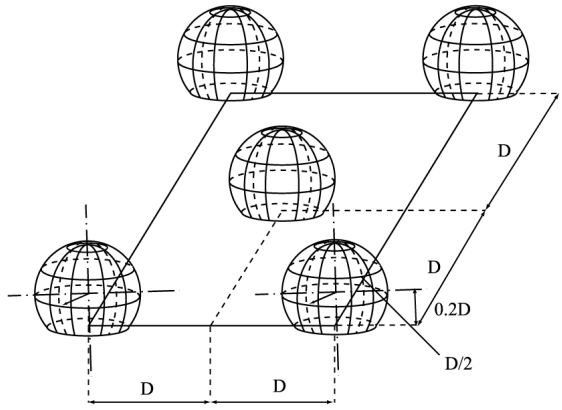


(b) Staggered arrangement

**Figure 2.**

The flow is assumed to enter the channel from a vertical section (plane *y-z*) placed six diameters upstream the the centres of the first column of spheres (Figure 2(a)). The velocity at the inlet is always assumed to be unity in magnitude, but its direction (angle of attack) has been allowed to vary. The flow direction at the inlet section, although always parallel to the vertical sides of the domain (*x-y* plane), has been varied with respect to the *x-z* plane as shown in Figure 3. Three different inlet directions have been studied with 0°, 10° and 20° angles of attack with respect to the *x-z* plane.

In all cases considered, no-slip velocity boundary conditions have been considered for horizontal bottom wall and solder ball surfaces. All other surrounding boundaries are assumed to be far field. In addition to the above flow conditions, different thermal conditions are prescribed on different boundaries. The solder ball surfaces are always assumed to be at a higher temperature ($T = 1$) than that of the incoming fluid ($T = 0$). All side boundaries are assumed to be adiabatic and at exist, free conditions are assumed (no temperature boundary conditions).

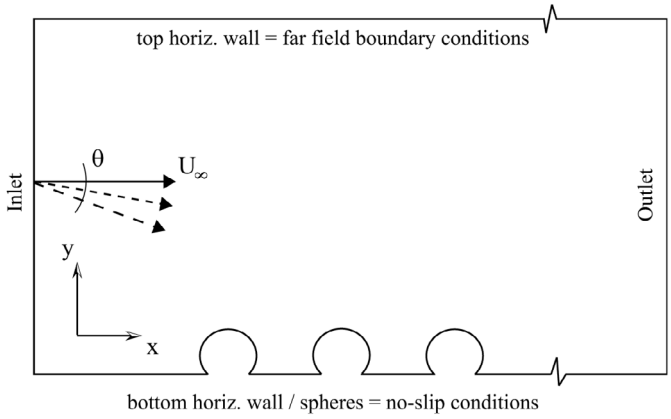


(a) Velocity boundary conditions at the inlet

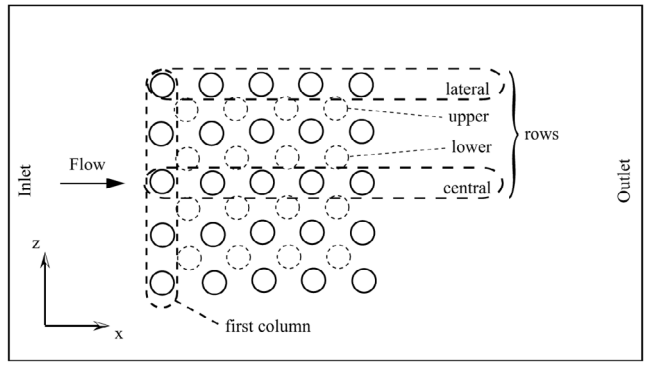


(b) Postion of the solder balls from above

**Figure 3.**
Planar sections of the computational domain (not scaled)

The domain presented above, in both configurations, has been subdivided into finite elements of unstructured meshes using an Delaunay type of mesh generator (Morgan *et al.*, 1999; Weatherhill *et al.*, 2001). All meshes are refined near the solid walls where strong gradients exist. The meshes used contained 250,372 nodes and 1,398,845 elements for the in-line arrangement and 237,911 nodes and 1,309,963 elements for the staggered arrangement. These grids where found to be satisfactory from a computational point of view after an appropriate mesh sensitivity analysis. Figure 4 shows an example of the surface mesh used for the in-line arrangement. The bottom adiabatic wall, where the no-slip boundary conditions are assumed, is refined near the spheres. For the staggered arrangement, the same density of nodes is assumed, and this results in a smaller number of nodes and elements.

## 7. Results and discussion

In this section, flow and heat transfer results obtained for the problem considered in Section 6 are presented. The results are mainly presented in terms of the heat transfer and fluid flow quantities of interest. The distribution of velocity and temperature is discussed in detail. The non-dimensional heat transferred from the spheres to the fluid has been calculated from the computed temperature distribution. In particular, the average Nusselt number for each sphere $\mathrm{Nu}_s$ is obtained, on the basis of its definition, from the following integral:

$$\mathrm{Nu}_s = \frac{1}{A_s}\int_A (\mathrm{Nu}_s)_p \, \mathrm{d}A = \frac{1}{A_s}\int_A \nabla T \cdot \boldsymbol{n} \, \mathrm{d}A = \frac{1}{A_s}\int_A \frac{\partial T}{\partial n} \, \mathrm{d}A \tag{31}$$

where $A_s$ represents the surface area of each solder ball ($s = 1, \ldots, 25$ for in-line and $s = 1, \ldots, 34$ for staggered arrangements) and $\boldsymbol{n}$ represents the out-going normal at each node on the surface of the spheres. The integral term written above has been

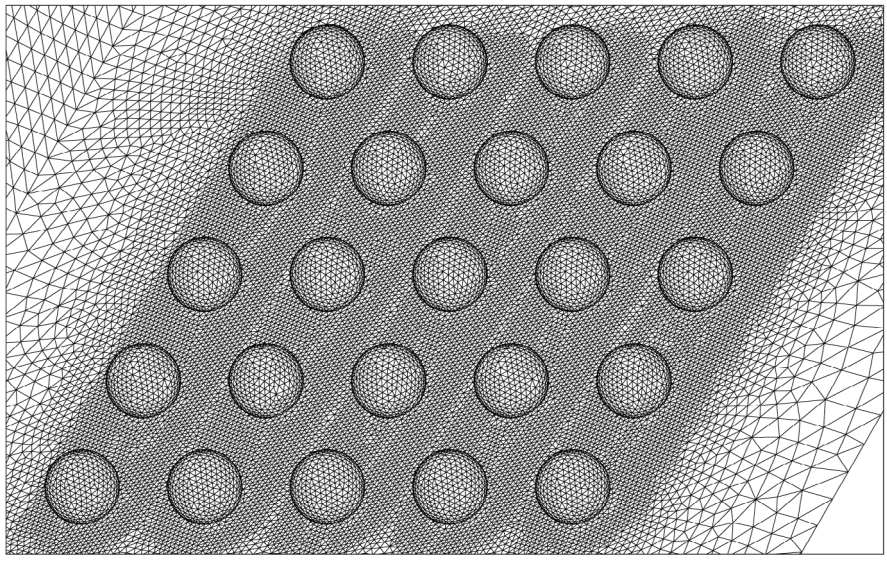

**Figure 4.**
The finite element mesh surface used for the in-line arrangement

calculated numerically by simply summing up the constant (linear elements) values of the gradient in each surface element multiplied by its area.

The value of the Nusselt number $Nu_s$, calculated for each solder ball has been calculated for different arrangements, Re and $\theta$ and compared.

*7.1 In-line arrangement*

In the in-line arrangement considered, 25 spheres have been equally distributed on the circuit board as shown in Figure 2. The isotherms calculated on a horizontal plane surface on which the balls are placed are shown in Figure 5. This picture shows the isotherms for Reynolds numbers from 100 to 300 and for different flow angles imposed at the inlet of the computational domain.

With zero angle of attack, the isotherm looks simple and uniform in the flow direction and convection from the ball cluster in the lateral direction is confined to a small thermal boundary layer. However, as the angle of attack is increased, the isotherms spread to a wider area around the cluster and showing a stronger convective mixing. At higher angle of attacks, the isotherms spread out and reach the side boundaries. This behaviour seen to has enhanced further as the Reynolds number is increased. It is also noticed that the symmetry with respect to the central row of spheres is preserved for all the angle of attacks and Reynolds numbers considered.

Although Figure 5 shows an idea of the qualitative patterns of temperature distribution, it gives very little information about the heat transferred from the balls to the fluid. In Figure 6 the average Nusselt number is shown for the central and lateral rows of balls (see Figure 3(b) for "lateral" and "central" rows). It should be noted here that the average Nusselt number for spheres in the row between "central" and "lateral"

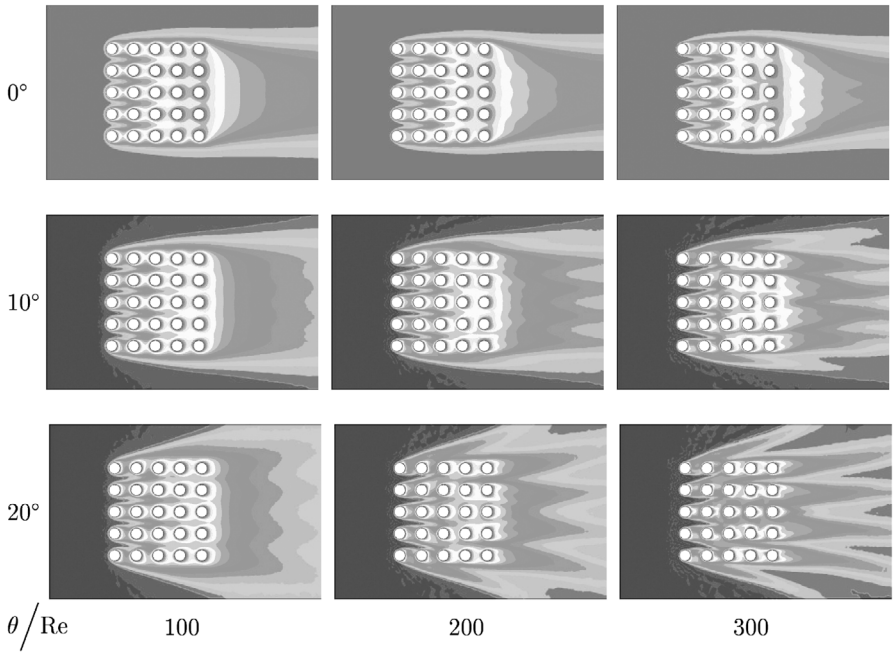


**Figure 5.**
Isotherms for different Re and inlet velocity angle for the in-line arrangement

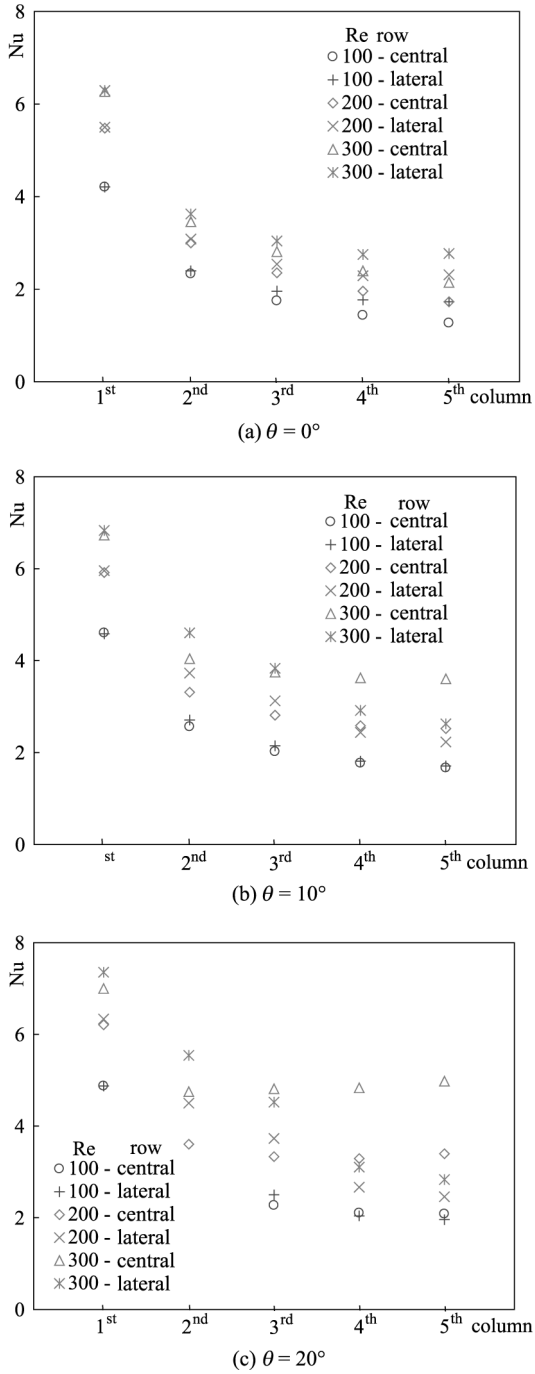


**Figure 6.**
Nusselt number for different Reynolds numbers and inclination angles

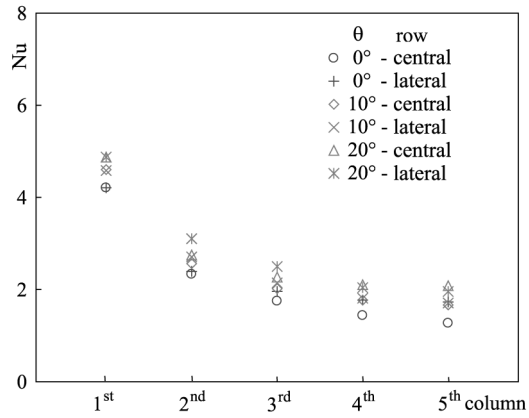


**Figure 7.**
Nusselt number for different inclination angles and Re = 100

rows are not shown in Figure 6 because it is practically the same as the values of the Nusselt number on the "central" row. From Figure 6(a) it is clear that a significant drop in heat transferred from the solder balls is noticed after the first column. A more uniform reduction in heat transfer is noticed from the columns of balls towards down stream. This is obviously due the flow obstruction caused by the columns of balls in the front. However, this effect tends to decrease after the third column. In fact, the fourth and fifth columns have practically the same values of Nu. As expected heat transfer rate from the lateral rows is much higher than that of the central rows.

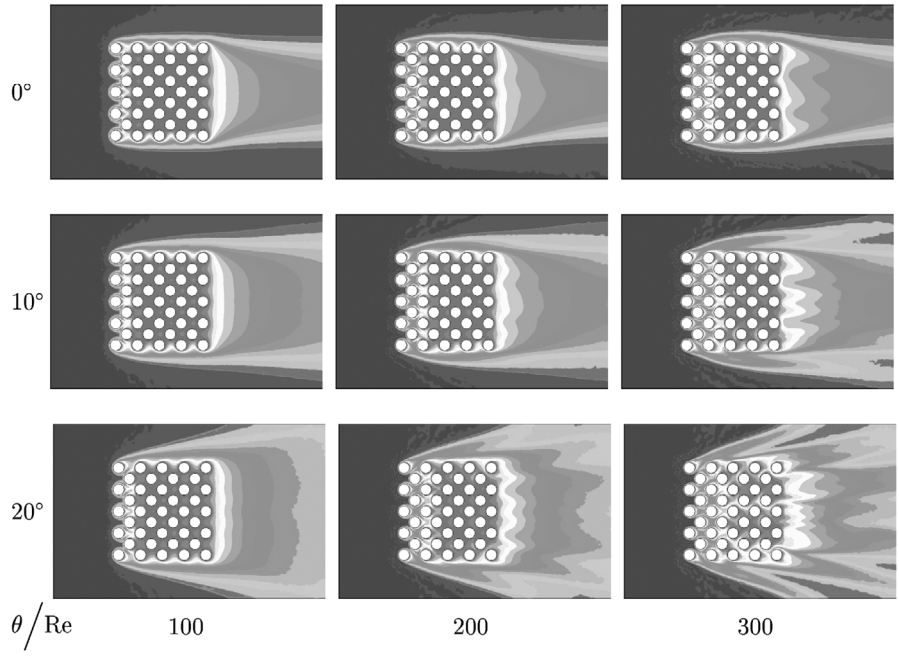


**Figure 8.**
Isotherms for different Re and inlet velocity angle respect to the horizontal plane for the staggered arrangement

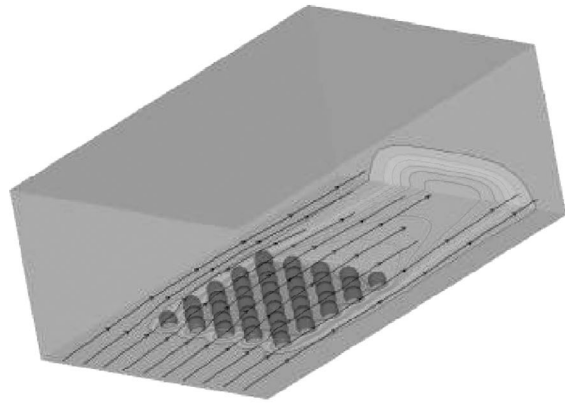

(a) Re = 100

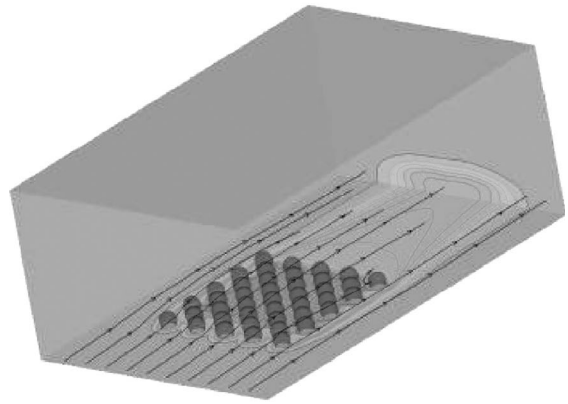

(b) Re = 200

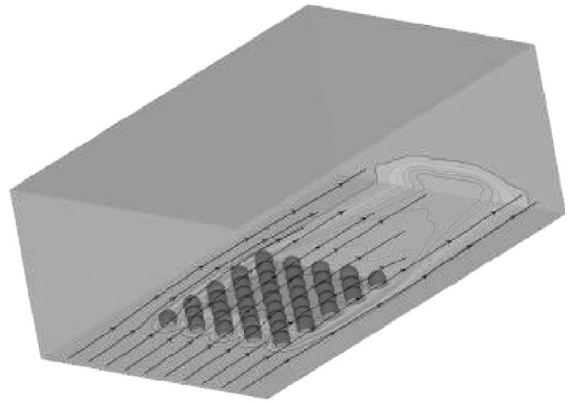

(c) Re = 300

**Figure 9.**
Isotherms for different Re and the inlet velocity parallel to the horizontal plane

At lower Reynolds numbers and higher angle of attacks, however, the difference in Nusselt number between the "central" and "lateral" rows are very small. In general, the increase in flow angle increases the heat transfer rate. It is due to the increase in the participation of balls at the middle of the cluster as seen from Figure 5. This effect becomes more relevant, especially for higher values of Re. This information about the influence of angle of attack can be very useful in this type of applications in which the central part of electronic devices tends to be usually the hottest.

The increase in heat transfer rate with increase in the angle of attack is also evident from Figure 7 in which the Nusselt number is plotted at Re = 100 for different angles of attack. In some cases the increase is more than 50 per cent.

*7.1.1 Staggered arrangement*. In the second arrangement considered, 16 more solder balls are added to those considered in the previous example. A sketch of the staggered arrangement is shown in Figure 3(b) for the sake of clarity. The boundary conditions are same as the in-line arrangement discussed in the previous sub-section.

In this case, the interaction between the spheres is even more pronounced, because of the higher degree of packaging obtained. In fact, the distance between the in-line balls is kept the same as the previous case, but more solder balls are inserted in the space that was left free between the balls.

Figure 8 shows the temperature contours (top view) for different Re and different angles of $\theta$ of the inlet flow. Figure 9 shows a sample three-dimensional figure showing both temperature distribution and stream traces for zero angle of attack and for different Reynolds numbers. It is seen that close packaging reduces the fluid penetration and thus, the spread of the temperature contours. In fact, temperature gradients in the zone occupied by the balls are very contained and this is shown by the uniform almost isothermal area at the centre of the packaging. The flow encounters several columns of balls in staggered arrangement and therefore, decelerates drastically after the first column. By increasing the velocity of the fluid, it is obviously possible to increase the temperature gradients between the balls and the cooling fluid. As shown in the Figure 8, for an angle of 0° the cool fluid penetrates more into the packaging as the velocity magnitude, and therefore, the Re increases. However, this is achieved with a large increase of the energy consumed to speed up the fluid (this energy grows at least with the square of the velocity). As in the case of in-line

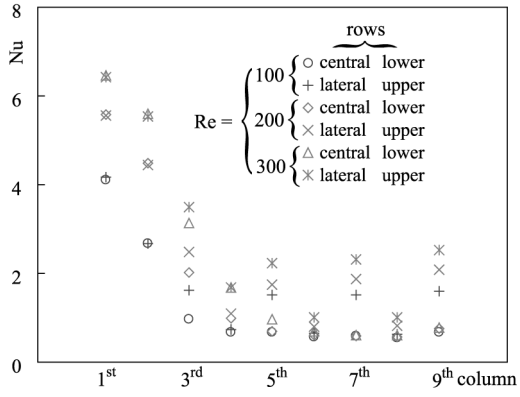


**Figure 10.**
Nusselt number for different Reynolds numbers and $\theta = 0°$

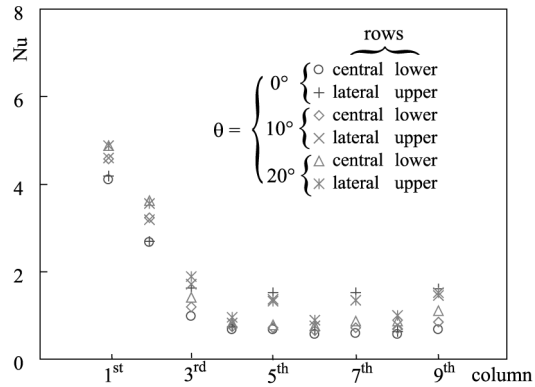


(a) $Re = 100$

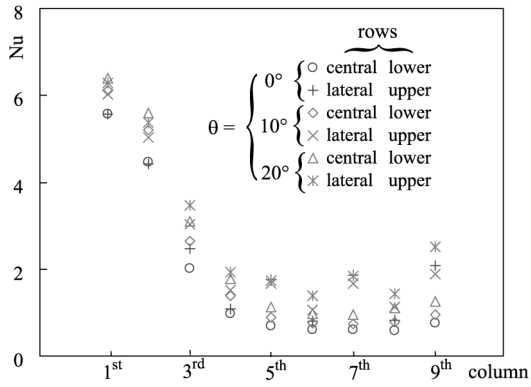


(b) $Re = 200$

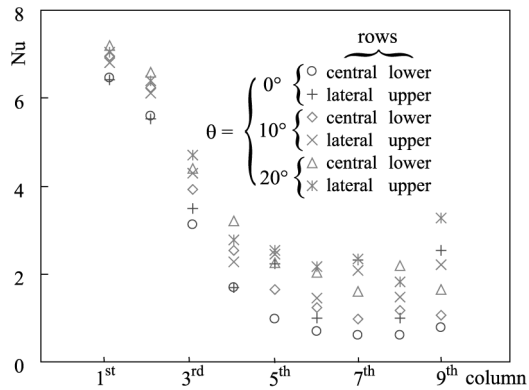


(c) $Re = 300$

**Figure 11.**
Nusselt number for different Reynolds numbers and inclination angles

arrangement, the fluid penetration increases with both Reynolds number and angle of attack. Note that for the same intensity of fluid penetration into the cluster, the staggered arrangement needs much higher Reynolds number and angle of attack than that of in-line arrangement.

The average Nusselt number variations with different Reynolds numbers and flow angles for staggered arrangement of the solder balls are shown in Figures 10 and 11. In these figures $x$-axis represents the column numbers of the ball cluster. For all legend details given in the figure, see Figure 3(b). The symbols used for "central" and "lower" rows are the same as balls from these rows do not fall onto the same column. For example, the "central" row balls fall onto the columns with odd numbers, but "lower" rows fall onto columns with even numbers.

As in the in-line arrangement the average Nusselt number obtained is smaller for the balls at the centre of the cluster. The front column, as expected, gives the highest heat transfer rate. As the angle of attack of incoming flow is increased, the participation of the balls within the cluster increases and thus, the heat transfer. However, the Nusselt numbers calculated are much smaller than that of the in-line arrangement for the same Reynolds number and angle of attack. This shows the effect of compact packaging.

## 8. Conclusions

The CBS scheme in its fully explicit form has been implemented and tested in three-dimensions for non-isothermal problems. A three-dimensional practical heat transfer problem has been successfully simulated using a fully explicit version of the CBS algorithm. The heat transferred from different arrays of solder balls, as may be found on a PCB, has been studied in the present work. The fully three-dimensional analysis has shown the influence of the arrangement and of the direction of the inlet flow on the heat transferred from the arrays of spherical balls used to describe the solder balls. In both cases of solder ball arrangements considered, it has been shown that, although the heat transferred can be increased by augmenting the inlet velocity, similar effects can be achieved by simply controlling the angle of incidence of the cooling fluid. The heat transfer rate from the solder balls increases by more than 50 per cent in some cases when the angle of incidence of the flow direction over the board is increased. This result could be used for new design of electronic cooling devices. However, further study is needed in this case to fully characterize the influence of the velocity direction and turbulence effects.

## References

Bar-Cohen, A., Watwe, A. and Seetharamu, K.N. (2001), "Fundamentals of thermal management", in Tummala, R.R. (Ed.), *Fundamentals of Microsystem Packaging*, Chapter 6, McGraw-Hill, New York, NY.

Chorin, A.J. (1967), "A numerical method for solving incompressible viscous flow problems", *J. Comp. Phys.*, Vol. 2, pp. 12-26.

Clift, R., Grace, J.R. and Weber, M.E. (1978), *Bubbles Drops and Particles*, Academic Press, New York, NY.

Comini, G. and Giudice, S. Del (1972), "Finite element solutions incompressible Navier-Stokes equations", *Num. Heat Transfer, Part A*, Vol. 5, pp. 463-78.

Dandy, D.S. and Dwyer, H.A. (1990), "A sphere in shear flow at finite Reynolds number: effect of shear on particle lift, drag, and heat transfer", *Journal of Fluid Mechanics*, Vol. 216, pp. 381-410.

Feng, Z.G. and Michaelides, E.E. (2000), "A numerical study on the heat transfer from a sphere at high Reynolds and Peclet numbers", *Int. J. Heat Mass Transfer*, Vol. 43.

Gresho, P. and Sani, R.L. (1999), *Incompressible Flow and the Finite Element Method*, Wiley, New York, NY.

Gülçat, Ü. and Aslan, A.R. (1997), "Accurate 3D viscous incompressible flow calculations with the FEM", *Int. J. Num. Meth. Fluids*, Vol. 25, pp. 985-1001.

Heindel, T.J., Incropera, F.P. and Ramadhyami, S. (1996), "Enhancement of natural convection heat transfer from an array of discrete heat sources", *Int. J. Heat Mass Transfer*, Vol. 39, pp. 479-90.

Löhner, R. (2001), *Applied CFD Techniques*, Wiley, New York, NY.

Malan, A.G., Lewis, R.W. and Nithiarasu, P. (2002), "An improved unsteady, unstructured, artificial compressibility, finite volume scheme for viscous incompressible flows: part I. Theory and implementation", *Int. J. Num. Meth. Engng.*, Vol. 54, pp. 695-714.

Massarotti, N., Nithiarasu, P. and Zienkiewicz, O.C. (1998), "Characteristic-Based-Split (CBS) Algorithm for incompressible flow problems with heat transfer", *Int. J. Num. Meth. Heat Fluid Flow*, Vol. 8, pp. 969-90.

Morgan, K., Weatherhill, N.P., Hassan, O., Brookes, P.J., Said, R. and Jones, J. (1999), "A parallel framework for multidisciplinary aerospace engineering simulations using unstructured meshes", *Int. J. Num. Meth. Fluids*, Vol. 31, pp. 159-73.

Nakayama, A. and Kuwahara, F. (2000), "Numerical modeling using microscopic structures", in Vafai, K. (Ed.), *Handbook of Porous Media*, Chapter 10, Marcel Dekker, New York, NY.

Nakayama, W., Behnia, M. and Soodphakdee, D. (2001), "Numerical modeling using microscopic structures", *IEEE Trans. Comp. Packag. Technol.*, Vol. 24, pp. 199-206.

Nithiarasu, P. (2002), "On the boundary conditions of the characteristic based split (CBS) algorithm for fluid dynamics", *Int. J. Num. Meth. Engng.*, Vol. 54, pp. 523-36.

Nithiarasu, P. (2003), "An efficient artificial compressibility (AC) scheme based on the characteristic based split (CBS) method for incompressible flows", *Int. J. Num. Meth. Engng.*, Vol. 56, pp. 1815-45.

Nithiarasu, P., Mathur, J.S., Weatherill, N.P. and Morgan, K. (2004), "Three-dimensional incompressible flow calculations using the characteristic based split (CBS) scheme", *Int. J. Num. Meth. Fluids*, Vol. 44, pp. 1207-29.

Ramaswamy, B., Jue, T.C. and Atkin, J.E. (1992), "Semi-implicit and explicit finite element schemes for coupled fluid thermal problems", *Int. J. Num. Meth. Engng.*, Vol. 34, pp. 675-96.

Rimon, Y. and Cheng, S.I. (1969), "Numerical solution of a uniform flow over a sphere at intermediate Reynolds numbers", *Phys. Fluids*, Vol. 12, pp. 949-59.

Shidore, S., Adams, V. and Lee, T-Y. (2001), "A study of compact thermal model topologies in CFD for a flip chip plastic ball grid array package", *IEEE Trans. Comp. Packag. Technol.*, Vol. 24, pp. 191-8.

Watson, S.P., Murray, B.T. and Sammakia, B.G. (2001), "Computational parameter study of chip scale package array cooling", *IEEE Trans. Comp. Packag. Technol.*, Vol. 24, pp. 184-90.

Weatherhill, N.P., Hassan, O., Morgan, K., Jones, J. and Larwood, B. (2001), "A parallel framework for multidisciplinary aerospace engineering simulations using unstructured meshes", *Engineering Computations*, Vol. 18, pp. 347-75.

Whitaker, S. (1983), *Fundamental Principles of Heat Transfer*, Krieger Publishing Company, Malabar.

Yuge, T. (1960), "Experiments on heat transfer from spheres including combined natural and forced convection", *ASME J. Heat Transfer*, Vol. 82, pp. 214-20.

Zhao, C.Y. and Lu, T.J. (2002), "Analysis of microchannel heat sinks for electronic cooling", *Int. J. Heat Mass Transfer*, Vol. 45, pp. 4857-69.

Zienkiewicz, O.C. and Taylor, R.L. (2000), *The Finite Element Method*, Vols 1-3, Arnold, London, UK.